ISSN 1063-7842, Technical Physics, 2018, Vol. 63, No. 9, pp. 1293–1299. © Pleiades Publishing, Ltd., 2018.
Original Russian Text © M.E. Sasin, V.I. Tushkanov, A.G. Smolin, P.S. Shternin, O.S. Vasyutinskii, 2018, published in Zhurnal Tekhnicheskoi Fiziki, 2018, Vol. 88, No. 9, pp. 1336–1343.

## PHYSICAL APPROACHES AND PROBLEMS OF DATA INTERPRETATION IN THE LIFE SCIENCES

# Polarized Fluorescence in Indole under Two-Photon Excitation by Femtosecond Laser Pulses

**M. E. Sasin[a,*], V. I. Tushkanov[a,b], A. G. Smolin[a], P. S. Shternin[a], and O. S. Vasyutinskii[a]**

[a] *Ioffe Institute, Russian Academy of Sciences, St. Petersburg, 194021 Russia*
[b] *St. Petersburg Academic University, St. Petersburg, 194021 Russia*
**e-mail: sasin@ffm.ioffe.ru*

Received January 23, 2018

**Abstract**—We have analyzed the decay of fluorescence intensity in indole dissolved in propylene glycol under two-photon excitation by linearly and circularly polarized femtosecond laser pulses in the wavelength range 475–510 nm. The dependences of fluorescence intensity $I_0$, anisotropy $r$, and parameter $\Omega$ on the excitation energy have been determined and analyzed. In particular, a nonmonotonic behavior of $I_0$ indicating the increase of indole excited state density in the excitation energy range above 5.1 eV and the anisotropy sign reversal due to the variation of the symmetry of indole vibronic states have been observed and interpreted theoretically.

**DOI:** 10.1134/S1063784218090189

## INTRODUCTION

The analysis of molecular fluorescence under two-photon excitation has been used for many years as one of important tools for investigation of the structure and dynamics of excited states of polyatomic molecules in gas and condensed phases, as well as biological structures [1]. Considerable advantages of the two-photon excitation technique over the single-photon one in medicine and biology are due to its high spatial resolution and the possibility of a deeper penetration into biological samples. Wide application of femtosecond lasers in multiphoton molecular spectroscopy allows one to implement noninvasive methods for investigation of the structure and dynamics of amino acids, enzymes, proteins, and other biomolecules [1, 2]. The theoretical basements of the method of two-photon excitation of molecular fluorescence were established by McClain, Callis, and others [3–6] who demonstrated that the polarization of fluorescence can be described by a set of molecular parameters, which decay exponentially in the conditions of isotropic interaction with solvent molecules with the characteristic excites state lifetimes $\tau_f$ and rotational diffusion times $\tau_{rot}$ describing the blurring of the excited molecule axes distribution. Within this approach, to use probe fluorescing molecules embedded in large biomolecules can be used for investigation of the biomolecule structure and dynamics in biological samples and living cells.

In our previous studies, a quantum-mechanical theory of molecular fluorescence exited by two-color two-photon (2C2P) laser pulsed in polyatomic molecules based on the spherical tensors approach has been developed [7, 8]. Earlier, this approach was successfully used for the treatment of a number of molecular dynamics problems related to the vector correlations in molecular photodissociation [9–13] and in inelastic molecular collisions [14]. General expressions describing the fluorescence intensity decay in asymmetric top molecules have been derived, where the part describing the polarization of all three photons involved in the photoprocess was separated from the part describing the dynamics of molecular excited states. The expressions allowed for considerable simplification of experimental data analysis and for development of a new method for extracting molecular parameters from experiment. This method was employed for experimental investigation of the processes emerging under the two-photon excitation of a number of molecules of practical importance: *n*-terphenyl, DMQ (2-methyl-5-tetrabutyl-*n*-quadrophenyl), indole, and NADN (nicotinamide-adenine-dinucleotide) [8, 15–18].

This work is devoted to the analysis of optical properties of indole ($C_8H_7N$) dissolved in propylene glycol based on the recording of polarized fluorescence under two-photon excitation by pulsed linearly and circularly polarized light from a femtosecond laser in the wavelength range 475–510 nm. Indole is a natural chromophore of an amino acide tryptophan, which is responsible to a considerable extent for fluorescence of proteins in the UV spectral range [2]. Due to considerable practical importance of tryptophan as a structural element of most proteins and its possible application as a molecular probe, a vast number of publications were devoted to the analysis of the dynamics

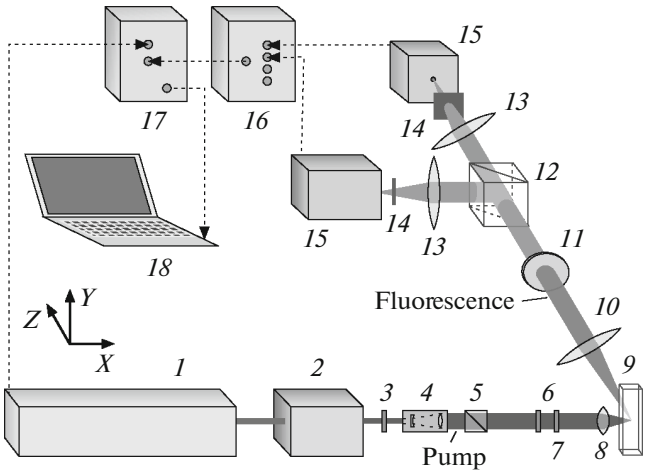


**Fig. 1.** Schematic diagram of experimental setup: (*1*) femtosecond laser; (*2*) frequency doubler; (*3*) λ/2 phase plate; (*4*) telescope; (*5*) polarization prism; (*6*) λ/2 phase plate; (*7*) λ/4 phase plate; (*8*) focusing lens; (*9*) absorption cuvette; (*10*) converging lens; (*11*) narrow-band interference filter; (*12*) Glan prism; (*13*) focusing lenses; (*14*) UV filters; (*15*) photodetectors; (*16*) router; (*17*) time-correlation single-photon (TCSP) analyzer; and (*18*) PC. Dashed lines indicate the directions of electronic signals.

of excited states of indole (see, e.g., [16, 19–22]). However, relatively low excitation energies (4.3–4.7 eV), which are equivalent to the effective excitation wavelength range of 265–295 nm, were used in the overwhelming majority of investigations.

In this paper, higher excitation energies related to the effective wavelength range of 265–250 nm were used. This resulted in population of highly excited vibrational states of the first two excited electron energy levels $^1L_a$ and $^1L_b$ of indole and low vibrational energy levels of the third electron excited state. By analysis of the fluorescence polarization, the intensity and anisotropy of two-photon population of indole vibronic states were studies in detail as a function of the excitation photon energy and polarization. It was found that anisotropy reverses its sign in the studied range of excitation. The indole excited state lifetime and the rotational diffusion time were also determined from experiment. The results obtained were interpreted using quantum-chemical ab initio calculations and the expressions for fluorescence intensity derived in our earlier investigations. We also developed a model of relaxation of excited electron-vibrational states of indole and showed that the observed behavior of the total absorption signal and its anisotropy as a function of the excitation energy can be satisfactorily described in the framework of the theory developed in the Born–Oppenheimer approximation. The determined values of the excited state lifetime $\tau_f$ and rotational diffusion time $\tau_{rot}$ were found to be in a good agreement with the results of our earlier works [16, 17] as well as with the results reported by other authors.

## 1. EXPERIMENTAL

In this paper, we used the technique for obtaining and processing of experimental results, which was developed in our previous works [7, 8]. Fluorescence in indole dissolved in propylene glycol was excited by a pulsed laser beam propagating along the *X* axis (see Fig. 1) and focused on a cuvette containing the solution. The mean laser beam power at the cuvette was 30 mW with a pulse repetition rate of 80.7 MHz and a pulse duration of about 150 fs. The laser beam was either linearly polarized along *Y* or *Z* axis or circularly polarized; the degree of polarization for all configurations exceeded 99.5%. The intensity of two fluorescence components linearly polarized along mutually orthogonal *X* and *Y* axes was detected by two independent photodetectors. Electrical signals from the photodetectors were recorded by a TCSP analyzer and then processed by a PC. The laser radiation wavelength was tuned in the range 475–510 nm that allowed us to study the dependence of the fluorescence parameters on the excitation energy.

The experimental setup is shown schematically in Fig. 1. The source of pump radiation contained a Mai Tai HP DS tunable pulsed femtosecond Ti : Sa laser (Spectra-Physics) and an Inspire Blue frequency doubler (Spectra-Physics). After frequency doubling, the laser beam passed through a λ/2 phase plate, a telescope, and a 10GL08 polarization prism (Newport) used for expansion and collimation of the beam to 4 mm in diameter and its attenuation. The mean laser beam power was controlled by a Nova (OPHIR) power meter. Then, the laser beam passed through λ/2 and λ/4 phase plates used for control of its polarization. The laser beam was focused by a lens (NA 0.3) onto the center of a quartz cuvette containing the solution of indole in propylene glycol with a concentration of 0.05 mol/L.

The fluorescence of indole molecules was collected by a lens and transformed into a quasi-parallel beam directed along the *Z* axis that passed through a FF01-390/SP narrow-band interference filter (Semrock) with a transmission band of 320–370 nm for intercepting scattered laser radiation. After passing through the interference filter, the fluorescence beam was split by a Glan prism into two components with mutually perpendicular polarizations parallel to *X* and *Y* axes. Each component passed through a UFS5 absorption filter and then was focused at the active areas of high-rate photodetectors based on PDM PD-050-CNC (MPD) avalanche photodiodes with a single-photon response half-width of 200 ps operated in the photon-counting mode. The signals from the photodetectors commuted with a PHR 800 router (PicoQuant) and were fed to a PicoHarp 300 time-correlation analyzer (PicoQuant) with a sampling rate of 4 ps, the data from which were fed to a PC for further processing.

## 2. EXPERIMENTAL RESULTS AND THEIR PROCESSING

In the experiment, the decay of two orthogonally polarized fluorescence components was recorded under various two-photon excitation conditions. The excitation conditions were varied by tuning the laser radiation wavelength in the range 475–510 nm and by changing the laser beam polarization. Therefore, three pairs of fluorescence decay signals were recorded at each excitation wavelength: two signals initiated by linear polarization of laser beam along $Y$ and $Z$ axes and the third signal initiated by the left-handed circularly polarized beam.

Since the fluorescence signals exhibited no anisotropy in the case of linear polarization of laser beam along the $Z$ axis within the detection scheme used in our experiment, these signals were used for determination of the coefficient $G$ in Eq. 3 that accounted for the difference between the sensitivities in the $x$ and $y$ detection channels. In addition, since the right and left circular polarizations of the laser beam led to the same fluorescence signals, we used only one (left) circular polarization.

Figure 2 shows typical experimental signals obtained under excitation of indole by laser radiation polarized along $Y$ axis and by circularly polarized radiation at 510 nm. The fluorescence signals with polarizations along $Y$ and $X$ axes are denoted as *1*, *2* and *3*, *4* for linear and circular polarization of the laser beam, respectively. In general, the fluorescence signal intensity in Fig. 2 is denoted as $I_{eef}$, where subscripts $ee = YY$, $XX$, and $LL$ indicate the polarization of the first two exciting photons, while subscript $f = x, y$ indicates the fluorescence photon polarization. Symbols in Fig. 2 are our experimental results and solid curves are the results of fitting with formulas (3)–(11) given below. Difference between the fluorescence intensities for different laser beam polarizations caused by different efficiencies of two-photon excitation with these polarizations. Difference between the intensities of fluorescence components polarized along $Y$ and $X$ axes at the same laser beam polarization was due to anisotropic distribution of the axes of excited molecules [1, 18]. The experimental data contain isotropic and anisotropic components with different decay times. The isotropic component of intensity under linearly polarized laser excitation can be presented in the form [1, 18]

$$I_1(t) = \frac{1}{3}[I_{YYy}(t) + 2I_{YYx}(t)]. \quad (1)$$

The anisotropic component can be expressed in terms of the fluorescence anisotropy as

$$r_1(t) = \frac{I_{YYy}(t) - I_{YYx}(t)}{I_{YYy}(t) + 2I_{YYx}(t)}. \quad (2)$$

In our experimental conditions, both quantities in Eqs. (1) and (2) undergo one-exponential decay with

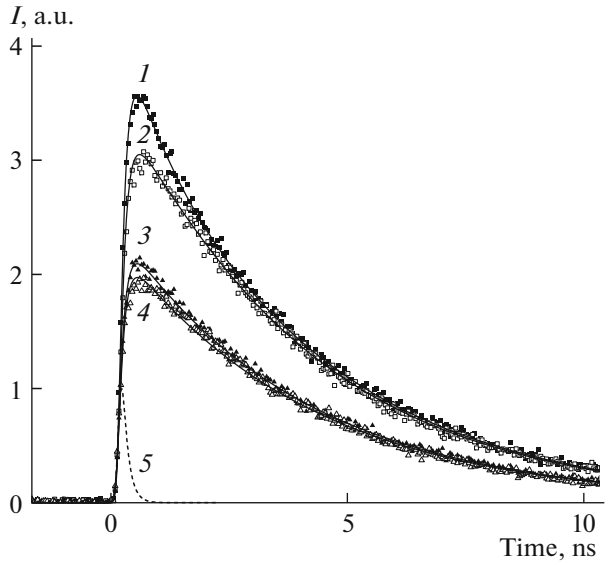


**Fig. 2.** Fluorescence decay signals under excitation by linearly and circularly polarized radiation at 510 nm. Symbols correspond to experimental data, solid curves are the results of fitting; *1–4* are the intensities of fluorescence components $I_{YYy}$, $I_{YYx}$, $I_{LLy}$, and $I_{LLx}$, respectively; (*5*) instrument response function IRF($t$) of the detector, $t = 0$ is the time of the laser pulse.

different characteristic times. For the isotropic component, this characteristic time was equal to the lifetime $\tau_f$ of the indole lowest excited state, for the anisotropic component it was equal to the rotational diffusion time $\tau_{rot}$ describing the anisotropy decay in the excited state axes distribution due to interaction with solvent molecules.

Because of the difference in the sensitivities in the $x$ and $y$ detection channels, the coefficient $G$, which is the ratio of the signals in the two channels in the absence of anisotropy, was introduced in Eqs. (1) and (2). For determination of the coefficient $G$, we used the ratio of the integrals

$$G = \frac{\int I_{ZZy}dt}{\int I_{ZZx}dt}, \quad (3)$$

where integration was performed to reduce noise.

Proceeding from Eqs. (1) and (2) and taking into account Eq. (3), the experimentally obtained polarization components of fluorescence can be presented as

$$I_{YYy}(t) = GI_1(t)[1 + 2r_1(t)], \quad (4)$$

$$I_{YYx}(t) = I_1(t)[1 - r_1(t)]. \quad (5)$$

The experimental data were processed using the technique similar to that described in [8, 16]. The instrumental detector response function IRF($t$) deter-

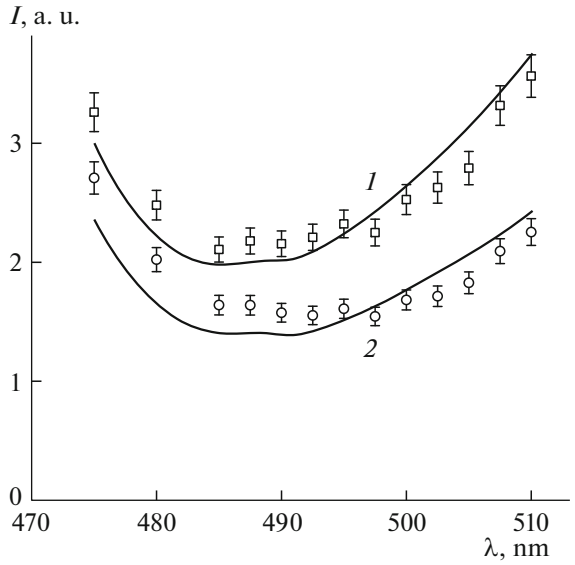


**Fig. 3.** Dependence of the isotropic component of the fluorescence intensity on the wavelength for linearly ($I_l$, curve *1*) and circularly ($I_c$, curve *2*) polarized excitation. Symbols correspond to experimental data, solid curves are the results of fitting.

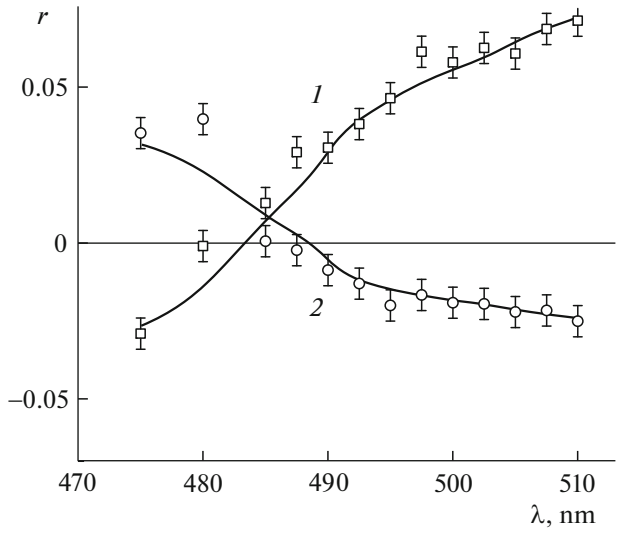


**Fig. 4.** Dependence of the fluorescence anisotropy on the wavelength for linearly ($I_l$, curve *1*) and circularly ($I_c$, curve *2*) polarized laser radiation. Symbols correspond to experimental data, solid curves are the results of fitting.

mined experimentally from the fluorescence signals shown by the dashed curve in Fig. 2.

The expressions used for approximation of the experimental data were of the convolution of Eqs. (4) and (5) with instrument function IRF($t$) and had the form

$$I_{YYy}(t) = G\int_{-\infty}^{t} \mathrm{IRF}(t')I_1 e^{\frac{t-t'}{\tau_f}}\left[1 + 2r_1 e^{\frac{t-t'}{\tau_{\mathrm{rot}}}}\right]dt', \qquad (6)$$

$$I_{YYx}(t) = \int_{-\infty}^{t} \mathrm{IRF}(t')I_1 e^{\frac{t-t'}{\tau_f}}\left[1 - r_1 e^{\frac{t-t'}{\tau_{\mathrm{rot}}}}\right]dt', \qquad (7)$$

where $I_1$ and $r_1$ are the time-independent values of the intensity isotropic and anisotropic components, respectively, in the case of linearly polarized excitation.

The approximation was performed in two stages. At the first stage, the lifetime $\tau_f$ of the excited state and intensity $I_1$ were determined on the basis of Eqs. (1), (6), and (7) by fitting. At the second stage, parameters $\tau_f$ and $I_1$ determined earlier were used as constants, and the values of $\tau_{\mathrm{rot}}$ and $r$ were determined on the basis of expressions (2), (6), and (7). For the circularly polarized excitation, indices $x$ and $y$ in Eqs. (1), (2), and (4)–(7) were interchanged, and the expressions for $I_1$ and $r_1$ were replaced by the expressions for $I_c$ and $r_c$, respectively.

The results of approximation are shown in Fig. 2 with solid curves. Using the procedure described above, the fitting parameters were determined at several wavelengths and different laser polarizations. In particular, we determined the values of characteristic times $\tau_f = 3.9 \pm 0.02$ ns and $\tau_{\mathrm{rot}} = 0.85 \pm 0.07$ ns, which were found to be independent of the excitation wavelength and were in good agreement with the results obtained in our previous works [16, 17].

The values of the isotropic components of the intensities $I_l$ and $I_c$ for linearly and circularly polarized laser radiation are shown in Fig. 3 as a function of the excitation wavelength. As can be seen, both intensities have maxima at the borders of the wavelength intervals under investigation and minima in the 480–500 nm range.

The dependences of the anisotropy parameters $r_l$ and $r_c$ on the excitation wavelength are shown in Fig. 4. It can be seen that the anisotropy parameters for linearly and circularly polarized excitations are out of phase with each other and change their signs approximately in the 482–484 nm interval.

Figure 5 shows the dependence of coefficient $\Omega$ characterizing the symmetry of the two-photon transition,

$$\Omega = \frac{I_{LL}}{I_{YY}}, \qquad (8)$$

on the excitation wavelength with linear and circular polarizations. As can be seen from the figure, this coefficient in the investigated spectral range is positive everywhere and increases monotonically with decreasing excitation wavelength (however, not attaining the critical value of $\Omega = 3/2$ indicating the presence of a not totally symmetric excited state [1]).

## 3. INTERPRETATION AND DISCUSSION

For interpretation of the experimental data, we used the results of quantum-mechanical calculations of the electronic structure of indole in the propylene glycol, which were described in our previous publication [17]. Some of these results are given in Table 1.

Two lowest excited electronic states of indole in Table 1 are well known and are usually denoted as $^1L_a$ and $^1L_b$ [1]. Minimum excitation energies $T_e$ of these states from the ground electronic state (4.32 and 4.56 eV) are given in the first two lines in Table 1. The transition dipole moments of one-photon transitions from the ground state to these electronic states, which are given in columns 4–6, lie in the molecular plane and are almost perpendicular to each other. The energy interval of two-photon excitation used in this study was substantially higher than these values, but lower than energy $T_e = 5.43$ eV of the next electronic state given in the third line of Table 1. Thus, the experimental signals represented in Figs. 3–5 are governed mostly by the population of highly excited ro-vibrational energy levels of the electronic states $^1L_a$ and $^1L_b$. At the same time, our analysis showed that in the given experimental conditions, a significant contribution to the short-wavelength part of signals in Figs. 3–5 was made by the population of the third excited electronic state in Table 1, which was possibly due to considerable (about 4 nm) broadening of the pulsed laser line used in the experiment.

The experimental signals given in Figs. 3–5 were interpreted on the basis of the theory developed in our previous publications [7, 8] using the data from Table 1 and taking into account the vibrational excitation spectra of indole and the femtosecond laser line profile. The vibrational excitation spectra for optical transitions from the ground electronic state to the excited electronic states under investigation were calculated in the Frank–Condon approximation taking into account the population of the ground-state vibrational levels at a temperature of 300 K. The calculations were performed on the basis of the GAUSSIAN package [23] with the parameters used earlier in [17]; the vibrational absorption spectra were determined taking into account the overtones and composite frequencies. The resultant vibrational excitation spectra had several peaks in the vicinity of the bottom of the electronic states and then decreases smoothly in amplitude with excitation energy. However, the complex structure of the vibrational excitation spectrum became almost indistinguishable after subsequent convolution of the vibrational excitation spectrum with the femtosecond laser line profile with a width of 4 nm.

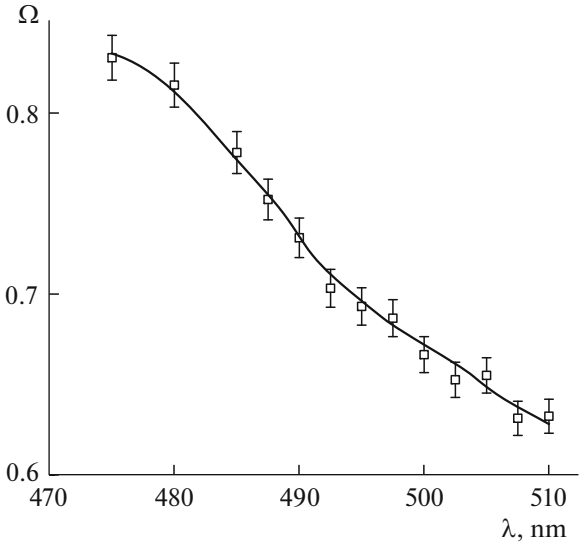


**Fig. 5.** Dependence of parameter Ω on the wavelength laser radiation. Symbols correspond to experimental data, solid curve is the results of fitting.

For fitting of the experimental data in Figs. 3–5, we used theoretical expressions obtained in our previous works [7, 8] based on the experimentally determined set of molecular parameters $M_K(R, R')$; the effect of the vibrational excitation spectrum was taken into account in the Born–Oppenheimer approximation. In the given experimental geometry, anisotropy parameters $r_l$, $r_c$, and Ω can be expressed in terms of the molecular parameters [8]:

$$r_{YY} = \frac{2}{5}\frac{M_2(0,2) + M_2(2,2)/\sqrt{7}}{M_0(0,0) + 2M_0(2,2)/\sqrt{5}}, \qquad (9)$$

**Table 1.** Energies of the lower excited electronic states and dipole moments of the excitation-induced transition from the ground state of the indole molecule in propylene glycol

| State | Symmetry | Energy | Dipole moment of transition, arb. units | | |
|---|---|---|---|---|---|
| | | | $X'$ | $Y'$ | $Z'$ |
| 1 | $A'$ | 4.32 | 0.5151 | −1.1421 | 0.0 |
| 2 | $A'$ | 4.56 | 0.8966 | −0.0290 | 0.0 |
| 3 | $A'$ | 5.43 | 2.7162 | −0.2314 | 0.0 |
| 4 | $A'$ | 5.91 | −0.8777 | 0.9732 | 0.0 |

**Table 2.** Values of parameters $M_0^e(2, 2)$, $M_2^e(0, 2)$, and $M_2^e(2, 2)$ normalized to $M_0^e(0, 0)$ and parameters $r_{YY}$ and $r_{RR}$ for each excited electronic state

| Parameters | Electronic state 1 | Electronic state 2 | Electronic state 3 |
|---|---|---|---|
| $M_0^e(2, 2)/M_0^e(0, 0)$ | $0.48 \pm 0.1$ | $2.33 \pm 0.31$ | $1.43 \pm 0.28$ |
| $M_2^e(0, 2)/M_0^e(0, 0)$ | $0.44 \pm 0.12$ | $-0.54 \pm 0.13$ | $-0.073 \pm 0.04$ |
| $M_2^e(2, 2)/M_0^e(0, 0)$ | $0.17 \pm 0.06$ | $-0.11 \pm 0.06$ | $-0.31 \pm 0.16$ |
| $r_{YY}$ | $0.15 \pm 0.3$ | $-0.084 \pm 0.02$ | $-0.036 \pm 0.014$ |
| $r_{RR}$ | $-0.058 \pm 0.012$ | $0.0076 \pm 0.02$ | $0.037 \pm 0.016$ |

$$r_{RR} = -\frac{1}{\sqrt{35}}\frac{M_2(2,2)}{M_0(2,2)}, \quad (10)$$

$$\Omega = \frac{3M_0(2,2)}{\sqrt{5}M_0(0,0) + 2M_0(2,2)}. \quad (11)$$

Molecular parameters $M_K(R, R')$ are described in detail in [7, 8], they contain complete information on the symmetry of two-photon excitation, which is defined in terms of the two-photon excitation and fluorescence tensors $S_{R\gamma}$ and $F$. The set of molecular parameters required for analysis can be determined directly from experimental data. In the Born–Oppenheimer approximation, two-photon excitation tensor $S_{R\gamma}$ can be written in the form

$$S_{R\gamma} = S^e_{R\gamma}\langle Q_{v'}|Q_{v''}\rangle + V_{R\gamma}, \quad (12)$$

where the matrix element in the angular brackets is the overlap integral of vibrational wavefunctions θ, while tensor $S^e_{R\gamma}$ is purely electronic.

Tensor $V_{R\gamma}$ in Eq. (12) contains higher-order terms of the expansion of tensor $S_{R\gamma}$ and characterizes the vibration-induced transitions that can be neglected in the given experimental conditions. The expression for the molecular parameters $M_K(R, R')$ for each electronic state can be written as

$$M_K(R, R') \approx M^e_K(R, R')|\langle\theta_{v'}|\theta_{v''}\rangle|^2, \quad (13)$$

where the terms $M^e_K(R, R')$ depend only on the electronic wavefunctions of the molecule.

To take into account simultaneous excitation of several electronic states, we performed summation over all corresponding molecular parameters. The fitting of experimental data was performed on the basis of Eqs. (2), (8), (9), and (11) by the least squares method with sequential determination of parameters $M_0^e(0, 0)$ and $M_0^e(2, 2)$ in terms of parameter Ω, then $M_2^e(2, 2,)$ was determined in terms of parameter $r_{RR}$, and finally $M_2^e(0, 2)$ was found in terms of parameter $r_{YY}$. The results of fitting are given in Table 2 and in Figs. 3–5.

The error of determination of the parameters $M_2^e(0, 2)$ and $M_2^e(2, 2)$ is somewhat larger than that for parameters $M_0^e(0, 0)$ and $M_0^e(2, 2)$ because the parameters $M_2^e(0, 2)$ and $M_2^e(2, 2)$ appear in the expression for the difference of in the fluorescence signals. As can be seen in Fig. 3, there are almost linear segments of the spectrum in the range of two-photon excitation exceeding 492 nm. These segments are successfully approximated by the contributions of the first excited electronic states, while the monotonous decrease in the fluorescence signal intensity in these regions is due to a decrease in population of highly excited vibrational states. At excitation wavelengths shorter than 492 nm, an increase in the intensity of two-photon absorption is due to the contribution of the lower vibrational states of the third excited electronic state. According to the results of calculation given in Table 1, the fourth excited electronic state lies much higher and does not contribute to the investigated spectral region. Therefore, our experimental results and interpretation confirm the contribution from the third electronic state to the fluorescence signals.

As can be seen in Fig. 4, the fluorescence anisotropy increases monotonous with the wavelength within the investigated spectral interval under linearly polarized excitation and decreases monotonous under the circularly polarized excitation. In this case, the changes in the anisotropy for linearly and circularly polarized pump radiation are out of phase, and anisotropy in both cases reverses its sign approximately at 485 nm. It should be noted that nonzero values of anisotropy were due to the anisotropic distribution (alignment) of the axes of excited molecules, which is observed for two-photon transitions induced by polarized laser radiation [1, 7] and is reflected in the polarization of observed fluorescence. The monotonous change in anisotropy upon a change in the excitation wavelength in both cases is due to a change in the symmetry of two-photon excitation tensor (12) of the second rank, $R = 2$, upon sequential population of the first, second, and third excited states of indole as described above. The out-of-phase change of the

anisotropy parameter values for linearly and circularly polarized excitation was due to the opposite signs of alignment of molecular axes for these two types of excitation [24].

As can be seen in Fig. 5, parameter $\Omega$ (see expressions (8) and (11)) as a function of the excitation wavelength decreases monotonous in the investigated spectral region, being positive everywhere, but not attaining the critical value $\Omega = 3/2$, which indicates the existence of a non-totally symmetric excited state [1]. Therefore, the results represented in Fig. 5 confirm the calculated data concerning the symmetry of the first three excited states of indole, which are given in Table 1.

## CONCLUSIONS

Thus, in this paper we studied the decay of polarized fluorescence of indole molecules dissolved in propylene glycol under two-photon excitation with linearly and circularly polarized femtosecond laser pulses in the wavelength range 475–510 nm. We have analyzed total absorption and anisotropy of two-photon population of electron-vibrational states of indole as a function of the energy and polarization of exciting photons. It was found that the anizotropy under linearly and circularly polarized excitations in the investigated spectral range vary in antiphase and reverse their signs. We have determined the lifetime of excited states and the rotational diffusion time. The results were interpreted on the basis of quantum-chemical ab initio calculations and analysis of the expressions for the polarization of fluorescence, which have been obtained by us earlier. We have built a model of the relaxation of excited electron-vibrational states of indole and have shown that the observed behavior of the total absorption signal and its anisotropy as a function of the excitation energy can be described satisfactorily on the basis of the theory developed in the Born–Oppenheimer approximation.

## ACKNOWLEDGMENTS

This study was supported by the Russian Science Foundation (project no. 14-13-00266).

## REFERENCES

1. Topics in Fluorescence Spectroscopy, Vol. 5: Nonlinear and Two-Photon-Induced Fluorescence, Ed. by J. R. Lakowicz (Kluwer Academic, New York, 2002).
2. A. P. Demchenko, *Ultraviolet Spectroscopy of Proteins* (Springer, 1986).
3. W. M. McClain, J. Chem. Phys. **57**, 2264 (1972).
4. C. Wan and C. K. Johnson, Chem. Phys. **179**, 513 (1994).
5. P. R. Callis, Annu. Rev. Phys. Chem. **48**, 271 (1997).
6. J. R. Lakowicz, I. Gryczynski, H. Malak, and Z. Gryczynski, Photochem. Photobiol. **64**, 632 (1996).
7. P. S. Shternin, K. H. Gericke, and O. S. Vasyutinskii, Mol. Phys. **108**, 813 (2010).
8. S. Denicke, K.-H. Gericke, A. G. Smolin, P. S. Shternin, and O. S. Vasyutinskii, J. Phys. Chem. A **114**, 9681 (2010).
9. S. K. Lee, R. Silva, S. Thamanna, O. S. Vasyutinskii, and A. G. Suits, J. Chem. Phys. **125**, 144318 (2006).
10. K. O. Korovin, B. V. Picheyev, O. S. Vasyutinskii, H. Valipour, and D. Zimmermann, J. Chem. Phys. **112**, 2059 (2000).
11. P. S. Shternin and O. S. Vasyutinskii, J. Chem. Phys. **128**, 194314 (2008).
12. V. V. Kuznetsov and O. S. Vasyutinskii, J. Chem. Phys. **127**, 044308 (2007).
13. D. V. Kupriyanov, B. N. Sevastianov, and O. S. Vasyutinskii, Z. Phys. D **15**, 105 (1990).
14. G. G. Balint-Kurti and O. S. Vasyutinskii, J. Phys. Chem. A **113**, 14281 (2009).
15. S. Herbrich, K. -H. Gericke, A. G. Smolin, and O. S. Vasyutinskii, J. Phys. Chem. A **118**, 5248 (2014).
16. S. Herbrich, T. Al-Hadhuri, K.-H. Gericke, P. S. Shternin, A. G. Smolin, O. S. Vasyutinskii, J. Chem. Phys. **142**, 024310 (2015).
17. M. E. Sasin, V. I. Tushkanov, A. G. Smolin, and O. S. Vasyutinskii, Opt. Spectrosc. **123**, 569 (2017).
18. O. S. Vasyutinskii, A. G. Smolin, C. Oswald, and K. H. Gericke, Opt. Spectrosc. **122**, 602 (2017).
19. B. Albinsson and B. Norden, J. Phys. Chem. **96**, 6204 (1992).
20. J. W. Hager and S. C. Wallace, J. Phys. Chem. **87**, 2121 (1983).
21. V. A. Povedailo and D. L. Yakovlev, J. Appl. Spectrosc. **75**, 336 (2008).
22. C. Kang, T. M. Korter, and D. W. Pratt, J. Chem. Phys. **122**, 174301 (2005).
23. M. J. Frisch, G. W. Trucks, H. B. Schlegel, et al., *Gaussian 09* (Gaussian Inc., Wallingford, 2009).
24. A. I. Chichinin, P. S. Shternin, N. Gödecke, S. Kauczok, C. Maul, O. S. Vasyutinskii, and K.-H. Gericke, J. Chem. Phys. **125**, 034310 (2006).

*Translated by N. Wadhwa*